ISSN: 0369-8963

Measurement of Hand-Arm Vibration Syndrome of an Agricultural Tractor Steering Wheel using Machine Vision System

R.GANESAN[1, 2*], G.SANKARANARAYANAN[1], M. PRADEEP KUMAR[3], V.K. BUPESH RAJA[1], S. SARAVANAN[4]

[1] Research Scholar, Research Supervisor, Professor, Department of Mechanical Engineering, Sathyabama Institute of Science and Technology, Chennai, 600119, India*
[2]Department of Mechanical Engineering, Sree Sastha Institute of Engineering and Technology, Chennai, India.
[3]Professor, Department of Mechanical Engineering, CEGC, Anna University, Chennai, 600025, India
[4]Department of Sports Medicine, University of Central Lancashire, Preston, United Kingdom

** Corresponding author: R.Ganesan*

Abstract:

The structure of an agricultural tractor is a structure without a suspension system to limit the vibrations generated by its engine. It exposed the entire body of an agricultural tractor operator to vibration. Thus, the body of the driver, constantly exposed to the vibration, becomes fatigued. This fatigue becomes a factor in the driver's inattention. The driver's body has transmitted to vibration through the tractor's seat, accelerator pedal, brake pedal, and steering wheel. Quantifying seat, accelerator pedal, brake pedal, and steering wheel vibrations is one of the most important factors in determining the cause of vibration and correcting it. The ISO 5349 standard lays down a guideline for the measurement and assessment of vibrations transmitted by the human hand. To meet the ISO 5349 standard, assess human exposure to hand-transmitted vibration and meet the human subjective comfort level. It must keep the vibration within a specified range. This study attempts to measure steering wheel vibrations through a new machine vision system using up-sampled cross correlation and a Discrete Finite Transform algorithm. In this study, it was impossible to calculate vibration in three axes from the video images recorded by the camera. According to ISO 5349-2, the vibration obtained on two axes multiplied by 1 to 1.7 to calculate the equivalent measurement for the vibration on the third axis. The results show that when the vibration is high; the errors are less and when the vibration is low, near zero, the errors range from 30 % to 50 %. But this study suggests that very low-level vibrations are unnecessary for vibration analysis. This study is not suitable for Nano-vibration measurement methods that measure fine vibrations.

Keywords: *Vibration measurement; object tracking; up-sampled cross-correlation; finite difference algorithm; template matching; Steering wheel; machine vision; Hand-Arm Vibration Syndrome*

INTRODUCTION

Most risky for agricultural tractor drivers are vibrations. The seat, frame, and controls convey engine vibrations to the driver's body. Vibrations can cause long-term health problems. Vibration measurement and evaluation are essential for safety precautions. Vibration tests on older tractors show that operating them for more than an hour a day exposes the operator to levels over the permissible limit. Employers must implement safety and organisational measures to reduce vibration levels. According to Indian standard IS/ISO 5349-1, 2001, Annex B, excessive hand-borne vibration impact impairs hand and arm motor function. According to research, 1.7% to 3.6% of workers exposed to hand-borne vibrations from vibrating machines. Hand-Arm Vibration Syndrome, also known as HAVS, is related to peripheral vascular, musculoskeletal, and neurological problems. Joint disorders and vascular illnesses are the most common occupational ailments caused by hand-borne vibration. "White" fingers are vascular diseases caused by machine-induced vibrations. According to Reynaud's occupational phenomenon origin, vibration-induced white finger (VWF) is a common occupational ailment in various nations. Raynaud's industrial origin divides hand-arm vibration syndrome into four categories based on the blanching procedure.

Vibration-exposed workers may develop tingling and numbness in their fingertips. These symptoms worsen in such conditions and can affect workability and everyday routines. In clinical trials among employees, vibration-stimulated fingers have less sensitivity than normal abilities, such

 https://doi.org/10.37896/pd91.4/91459

ISSN: 0369-8963

as tactile heat feeling and vibration perception. Over 80% of manual and machine workers have peripheral neuropathies, according to epidemiological studies. Studies indicate vibrations from vibrating machinery produce vacuum and fluid clots in the wrist bones. Workers with machines below 50 Hz have higher wrist and elbow arthritis. Medium and high-frequency machine operators suffer with Keinbock's disease (Malaysian lunate) and scaphoid pseudoarthrosis. Eye examinations reveal that workers working on machines with extra vibration affected with bone injuries, local pain, edoema, joint stiffness, and other bone problems. Long-term vibration causes muscle weakening, arm and leg pain, handgrip weakness, and weariness. Muscle tendons and tendons swelling, Dupuytren's contracture of the upper limbs, palmofacial tissue disease, etc. are ailments produced by persistent vibration in vibration-exposed employees. Russian and Japanese researchers revealed that workers with vibration-induced white finger illness had significantly worse hearing for their age. Vibration-induced vasoconstriction prevents blood from reaching the inner ear. The workers suffered peripheral illnesses and cerebral dysfunction. Continuous vibration causes weariness, headaches, irritability, sleeplessness, and impotence.

The root-mean-square (rms) frequency-weighted acceleration, given in meters squared per second (m/s2), is the main measurement used to indicate the magnitude of vibration. Frequency weighting Wh that explains the relative importance of different frequencies in causing hand damage. The resonance has defined as the total value, ahv, and the root-sum of the squares of the three component values.$a_{hv=\sqrt{a_{hwx}^2+a_{hwy}^2+a_{hwz}^2}}$ Eqn (1)

Where, a_{hwx}^2 , $a_{hwy,}^2$ a_{hwz}^2 are frequency weighted rms acceleration quantity in x, y and z directions respectively.

Three-axis vibration is not always quantifiable. It measured if just one or two is because of any constraints, include the largest, where this could identify. It may do total vibration estimation by multiplying the vibration axis by 1.0 to 1.7, as per ISO 5349-2. Vibration total value and daily exposure duration define daily vibration exposure. It must express the daily vibration exposure as the 8-h energy-equivalent frequency-weighted vibration total value, ahv (eq,8h), as illustrated by the equation: (2). For simplicity, ahv(eq,8h) has abbreviated as A(8).

$$A(8) = a_{hv}\sqrt{\frac{T}{T_O}} \quad \text{Eqn (2)}$$

Where T is total vibration exposure regarding ahv and To is 8 hours. If the daily vibration exposure includes operations with varying vibration magnitudes, then A(8) must be determined using equation(3)

$$A(8) = \sqrt{\frac{1}{T_o}\sum_{i=1}^{n} a_{hvi}^2\ T_i} \quad \text{Eqn (3)}$$

Where, a_{hv} is the vibration total value for the i^{th} operation, n is the number of individual vibration exposures, T, is the duration of the i^{th} operation. [1]

S. Gnanasekaran et al. tested steering wheel vibration in the lab. They compared test results to ISO 5349-1 and BSIA 6842. A lab-based test that evaluates the steering wheel frequency weightings (Ws) detail. Potholes, roll strips, street stones, upkeep gap covers, extension joints, country road, city road, and motorway were the eight driving situations studied. They each used a steering wheel-mounted accelerometer. Each had 8-60 seconds. The rotational framework's steering wheel rig comprised a 325mm aluminum wheel coupled to a steel shaft with bearings and an electro-dynamic shaker. The coefficients of assurance suggest that either frame of frequency weighting (Wh or Ws) delivers a more precise measure of human felt intensity than unweighted increasing speed, which provided comparable results. Wh and Ws reading differences were small, this needs explanation. [2]

B. Cvetanovic et al. indicate a Serbian company's estimate of whole-body tractor vibration exposure for drivers (IMT 533, IMT 539, IMT 558 and IMT 560). Using an HSE whole-body vibration calculator and evaluating drivers' occupational safety. ISO 2631-1:1997 and ISO

 https://doi.org/10.37896/pd91.4/91459

ISSN: 0369-8963

5008:2002 are the most common vertical acceleration standards, depending on magnitude, frequency, and duration. Relevant standards provide acceleration as a vibration measurement and assessment characteristic corrected by a frequency-weighting function. • For 0.5m A (8) >1.15 m/s2 (IMT 560), employers must reduce vibration, alert employees of vibration-related concerns, and allow them to undergo preventative medical exams.• Implement procedures to protect personnel against A (8) > 1.15 m/s2 (IMT 539, IMT 558), including medical checks. [3]

Morioka et al. evaluated steering wheel grip force and vibration frequency. A 12-person investigation demonstrated identical comfort contours for vertical hand vibration with three grip tensions. It calculated the amplitude of steering wheel vibration at seven frequencies (4 to 250 Hz) and a variety of vibration magnitudes (0.1 to 1.58 ms-2 r.m. s). The comfort contours altered with vibration magnitude, demonstrating that frequency weighting should include vibration amplitude. Increased grip force at low magnitudes increased comfort contour frequency dependency and sensitivity at high frequencies. Pacinian and non-Pacinian tactile channels may explain the results. [4]

This research offered a novel approach for analysing hand-arm vibration (HAV) in Malaysian Army three-ton truck steering wheels based on vehicle speed using a regression model and a statistical analysis technique called Integrated Kurtosis-Based Algorithm for Z-Notch Filter Technique Vibro (I-kaz Vibro). Paved, and gravel roads for test. The vibration analyzer analysed HAV exposure. I-kaz Vibro was used to analyse vehicle speed and data dispersion to determine HAV levels. Driver's HAV analysed using I-Kaz Vibro coefficient (Zv), display, and daily vibration exposure A (8). More scattering on I-Kaz Vibro displays Zv and A(8) are rising. Model and Zv visualisations predicted HAV exposure. Regression model: Zv increased with vehicle speed and HAV exposure. Comparing expected and measured noise exposures for model validation indicated a good agreement. Using a regression model, steering wheels can readily assess HAV risk. [5-6]

Janczur suggested employing steering and body vibration analysis to detect imbalanced wheels. This research examines how an imbalanced front wheel affects steering system vibration, the steering wheel, and the vehicle body. First, it tested a vehicle with balanced wheels on smooth asphalt. In phases, the front wheel's weight increased by 10, 20, 30, 40, and 60 g. Wheels balanced using Hunter GSP 9700. 100 Hz vibration system, VBox, Spider 8, computer, acceleration sensors, and wheel dynamometric. Vibrations from wheel imbalances can damage the suspension and steering wheel, thus it's crucial to recognise them. Real vehicle acceleration and speed are based on CAN bus data, chassis component knowledge permits data interpretation, and tyre monitor generates uncommon conditions or break disc brake misalignment. This monitor helps maintain the wheels' suspension and tyre life. [7]

Tang et al. studied multinode joint vibration control for a commercial vehicle's steering wheel. This article presents a multinode joint vibration control technique (MDVC) based on steering wheel vibration. Based on the steering wheel's vibrating patterns, the vehicle was separated into nodes. The steering communication system was divided by vibration path and direction. Researchers evaluated vibration at connection nodes in the steering subsystem, chassis, mounting subsystem, and Powertrain subsystem. A passive vibration test determined which sub-structure causes steering wheel anomalous vibrations. In an airless, dry environment, test data collecting equipment includes a 24-bit CPCI, electrical measurement computer, and tri-axial accelerometers. Triaxial accelerometers vs. FEM-based multinode joint vibration control (MDVC). Test results demonstrate the revised procedure minimised steering wheel vibration. [8]

M. Wandor et al. offered strategies and components for reducing steering gear vibration. It measured horizontal and vertical steering system vibrations. Vibrations can be directed in different directions or torques to probe sensors. The study examines steering gear housing vibrations. RMS values compare vibration energy directional distribution estimators. It used a quick Fourier transform to determine steering gear vibration frequency. Vibration analysis provides steering gear defect diagnosis and backlash analysis. [9]

 https://doi.org/10.37896/pd91.4/91459

ISSN: 0369-8963

To analyse commercial vehicle steering system vibrations, the natural frequency distribution must be detected. To determine vehicle component resonance frequency, it tested an unloaded commercial vehicle's high-speed resonant frequency. It examined the suggested integrated structural improvement using finite-element analysis and model testing. The results showed the stability of the combined approaches and that the enhanced steering structures' natural frequency and vibration amplitude changed. It compared regular steering vibration with optimised steering vibration. Improved steering wheel reduces vibration 13-55% After identifying the source of vibration, the optimum composite system increases the structure's rigidity and dampens the intermediary receiving components to isolate the vibration. Improved modelling and integrated analysis, integrating finite-element analysis and model testing, reduces steering wheel vibration and confirms experimental and simulation findings. [10]

The test conducted to determine the amount of vibration transmission in three axes (horizontal X, lateral Y and vertical Z) to the seat drive tractor, vector sum of vibrations in the seat drive tractor and daily vibration exposure (8 hours), and vibration in the steering tractor. Its measured heart rate, systolic and diastolic blood pressure and temperature in all the drivers before and after using the chisel plow in dynamic plowing. Soil moisture is two parts dry and wet with 16 to 19% moisture at tillage. The three drivers tractor (D1, D2 and D3) represent the third factor. The experiment comprised three replicates of each of the 18 treatments. Lutron Vibration Meter (Lutron VB - 8201HA) serial number (Q405638) manufactured in Taiwan is used to detect vibration levels. The effect of soil type, tractor speed and driver interaction measured on vertical (X, Y, Z) vibrations in a seat tractor. Increasing the speed tractor increases the vibrations in the seat tractor (longitudinal X, lateral Y and vertical). Correlation between tractor speed and drivers on daily vibration exposure (8 h) in seat tractors. Vibration levels in the seat and steering wheel of a tractor with eight hours of daily vibration exposure compared favorably with global penetration levels. All the tractor drivers had an increased heart rate after the experiment. All drivers had normal systolic and diastolic blood pressure, but it slightly elevated the temperature in the driver’s body. [11]

This project examines tractor steering wheel vibration. It identifies the problem's fundamental cause by designing and analysing the steering system to research hand arm vibration syndrome (HAVS). Through a mathematical model of steering wheel vibrations and FEA software simulation, it compared the estimated vibrations to acceleration sensor-measured vibrations. Acceleration signals (Time in seconds vs r.m.s in m/s2) at the steering wheel in X, Y, Z directions calculated. Acceleration signals (time in seconds Vs rms value in m/s2) of the steering box during operation. Vibrations are especially damaging. Continuous vibration levels recorded and evaluated to determine driver safety risk. Hand-arm vibration acceleration ranged from 4.1 to 3.1 m s-2 across the study's operations (HAVS). [12]

This work introduces MIAM to analyse vibration acceleration transfer. Calculate vibration acceleration transfer rates throughout the transmission line to discover probable seismic fault zones. The most likely fault region extracted by node position. By focusing on the steering system's overall vibration and eliminating vibration interference amongst related systems, the model's accuracy confirmed. Using FEA, model analysis of the simulation model, and material model of the extracted steering system model, it was determined that the model frequency of a certain order frequency of the steering system is close to the engine, thus facilitating vibration resonance caused by the excitation frequency. Original steering vibration wheel acceleration signal versus upgraded steering wheel. Compare the original and improved total weighted acceleration vibration signal at the steering wheel. The upgraded steering wheel vibrates. Based on the retrieved steering model, a structural development model comparison study validated the suggested strategy. The results reveal that the solution reduced steering wheel vibration amplitude and provided a reference for similar engineering difficulties. [13]

 https://doi.org/10.37896/pd91.4/91459

ISSN: 0369-8963

This document provided studies on steering wheel vibration in two-wheel drive tractors, observed tractor vibrations. Driver hand vibrations detected at idle and full load. It calibrated the vibration meter (VB-8201HA) for each reading. During the test, vibration levels from the steering wheel to the driver's hand exceeded ISO 5349-1: 2001. Taking breaks every two to four hours after starting work minimised long-term vibration concerns. [14]

This project solved tractor-wheel vibration difficulties. Design and analysis of control systems help discover problem causes. Tuned mass dampers reduced vibration. MATLAB Simulink with base excitation was used to analyse various damping materials for vibration reduction. Researchers measured steering wheel and steering box vibration using an FFT analyzer. Using an electrodynamic shaker to measure vibration using a damper. FFT analyzer vibration with and without damper measured from MATLAB Simulink two-DOF model. The damper reduces steering box vibration by 44.76%, steering wheel vibration by 63.97%, and total daily vibration and peak acceleration by 54.49% and 63.77%, respectively. The 2-DOF mathematical model and MATLAB simulation accurately predicted steering vibration. [15]

This paper investigated the vibration of a commercial vehicle's steering assembly and simplified its harmonics. The study compared commercial vehicle steering assembly vibration and optimization. This work developed a mathematical model to aid in understanding steering assembly design and material needs. The lumped-parameter technique models discrete mass, elastic, and damping elements as a spring-mass system, resulting in ODEs. Elastic and damping elements linked distinct masses. Model validity depends on several aspects. Add only enough components for natural vibrational modes and frequencies to save processing time. Using lumped parameters, this work constructed a vibrating steering wheel assembly. The method was validated using a real-world vehicle, and CAE analysis findings correlated by 45%. A method for determining commercial vehicle steering displacement and acceleration designed and assessed. [16]

This research provided a new way to isolate a system from sinusoidal and random vibrations. The experiment revealed that using metal-rubber vibration isolation pads reduced the vibration amplitude. Four metal-rubber vibration isolators were used between the steering wheel and the diverter. The static test calculates the vibration isolation and vibration damping capacity by measuring the compressive and relative elastic forces of metal rubber pads. Isolation performance and performing damping characteristics and its vibration analysis studied. This study established a method to use a fine metallic rubber damping cushion to reduce the excessive vibration amplitude of the steering wheel when the engine rotates at high speed. [17]

A prototype hydraulic steering system's critical point stress was evaluated to identify wheel loader steering vibration. AMESim designed and analysed a prototype steering system to find vibration causes. Simulation and loading testing optimised the cushion valve design. It used theoretical analysis and simulation to assess the cushion valve's effect on hydraulic steering. To save operator effort and time spent moving the steering wheel, shorten the working cycle, and enhance efficiency. Lateral acceleration rises. The rotary valve port opens quickly as the steering starts, producing a shock from the rapid flow of hydraulic oil from the pump. Tires and vehicle shock absorbers deform inertially when deformed. Anti-vibration valves lessen starting shock and pressure fluctuations. [18]

In compliance with ISO 5349, the intended to reduce vibration by detecting and analysing caused vibrations in the human hand and examining the human's subjective response. It contrasted three rounds of Finite Element Analysis employing modal frequency response analysis. The tractor's frequency response in X, Y, and Z directions compared and weighted RMS values to the platform's development, which was verified by simulation and testing. Vibration testing and subjective comparisons justified the finite element model iteration. [19]

 https://doi.org/10.37896/pd91.4/91459

ISSN: 0369-8963

This research report shows that increasing steering component stiffness without increasing weight is difficult, and elastomeric dampers are the best approach. It has developed five steering concepts. Using the assessment matrix, the most efficient and cost-effective concept chosen and evaluated with MATLAB as a two-degree-of-freedom system. It reduced vibration to acceptable levels. Elastomeric dampers minimise vibration. [20]

This study uses EU Council directive 2002/44/EC as a research criterion. It constructed six criteria using a design evaluation matrix. Two ideas and a two-degree-of-freedom (two-DOF) technique devised to determine steering vibrations from the engine using MATLAB expressions. A design evaluation matrix included six elements. It will develop these two concepts. Axial dampers reduce vibration amplitudes better than radial dampers. [21]

This research focuses on isolating the steering wheel of an agricultural tractor to reduce vibrations. It utilised materials and mechanical linkages in isolation to absorb and reduce engine vibrations. It measured vibrations in the steering wheel using established test procedures and software. The steering wheel vibration measured with and without damping and it compared the results. This study of various elastomeric materials revealed that Polyurethane is an effective axial damper material. [22]

Five tractors with good vibration control were studied. Tri-axial frequency-weighted acceleration data and running speed values were also acquired. Standard working conditions were used. The axis determines the risk to the operator from ploughing and harrowing roll. Cross-sectional risk for operator. Oddly, rural road translations determine vertical axis exposure. Tractor performance is greatly dependent on working conditions, hence absolute rankings are impossible. [23]

It tested the steering wheel's vibration. CATIA V5 generated the 3D steering model. Model analysis uses ANSYS19.2. It'll be impact-tested. Analytical and experimental results were compared. Carbon fiber reduces steering wheel weight by 60%. Carbon fiber steering wheels have a greater natural frequency than conventional ones, therefore excessive torque is less painful on the driver. [24]

By allocating a known real-world dimension to a preset image area, this research proposal estimates the scaling factor. For superior template matching using the improved Up-sampled Cross Correlation (UCC) approach, a new white sticker with known dimensions and a coloured dot stuck to an object's surface. It calculates vibration measurement using the Finite-Difference Algorithm (FDA), a computer vision system with a macro lens sensor that can record images at close range without compromising displacement measurement from video frames. A typical vibration measurement equipment verifies the results with great precision. [25-26]

This study highlights the expanded use of machine vision systems for the following purposes: Create a simple thermal imaging device that uses hot air to generate smooth thermal images Using a proprietary deep learning system trained on a defined sample of thermal pictures, classify wounded and healthy mango. The goal was to explain the modest fluctuation in mango lesions by computing the gray-level co-occurrence matrix (GLCM) value of thermal images acquired on consecutive days after bruising. [27]

High-performance cameras capture field images, which are subsequently analysed on a computer to measure strain, displacement, and tilt. After processing, dynamic features, such mode form, frequency, acceleration, and it can retrieve damping ratio. Researchers calculate the effect of line [28, 29].

 https://doi.org/10.37896/pd91.4/91459

ISSN: 0369-8963

This new research proposal aims to calculate hand arm vibration through machine vision, in a non-tactile way. Through this, the vibrations occurring in the tractor steering wheel can calculate and the maintenance strategies can possible so that those vibrations do not harm the hands of the tractor operator. This research proposal is based on the previous studies of the same researchers, aiming to improve the results of previous research.

PROPOSED MACHINE VISION SYSTEM

Vision sensors compare template displacements. Several research publications suggest a template-matching approach to discover a point's relative position in image frames. mm/pixel should compare real-world and video frame dimensions. Zhang's approach [38] reduced camera calibration and scaling distortion.

Scaling Factor

$$= \frac{\text{Real world dimensions on the surface ofthe object}}{\text{Pixel length of image plane}}$$

$$= \frac{\text{Camera to object distance}}{\text{Length of focus}} \times \text{Pixel size in } \left(\frac{\text{mm}}{\text{pixel}}\right) \qquad \text{Eqn (4)}$$

Improved Up-sampled Cross-Correlation Algorithm

Many research articles advocate the enhanced Up-Sampled Cross-Correlation (UCC) algorithm to calculate structural displacement in the x and y axes. The video frame picture (x, y) of size MxN will be matched with the key-frame template (x, y), which has a known dimension paper sticker with a colour dot to ensure errorless RGB matching. The mean RGB brightness was measured to track the paper sticker marking the video frames' blue colour. The template match changes colour and shape at a set interval. [25, 26]

Finite-Difference Algorithm for Vibration Measurement

Many research articles advocate the enhanced Up-Sampled Cross-Correlation (UCC) algorithm for calculating structural displacement in the x and y axes. The video frame picture (x, y) of size MxN will be matched with the key-frame template (x, y), which has a known dimension paper sticker with a colour dot to ensure errorless RGB matching. It measured the mean RGB brightness to track the paper sticker marking the video frames' blue colour. The template match changes colour and shape at a set interval. [25, 26]

Acceleration:

$$aXj = \frac{(2\times X(j+2) - X(j+1) - 2\times X(j) - X(j-1) + 2\times X(j-2))}{(7\times \nabla t^2)} \qquad (5)$$

$$aYj = \frac{(2\times Y(j+2) - Y(j+1) - 2\times Y(j) - Y(j-1) + 2\times Y(j-2))}{(7\times \nabla t^2)} \qquad (6)$$

where j- is the number of steps, aXj is the x-direction acceleration at j, and aYj-is the y-direction acceleration. X and Y are displacements in the x and y directions.

EXPERIMENTAL SETUP AND METHODS

Experimental Model and setup

Velocity and acceleration computed by using the sub-pixel cross-correlation value over a template. It compared machine vision acceleration findings to those of an integrated electronics piezo-electric (IEPE) accelerometer sensor, SIRIUS® MINI interface, and Dewesoft NVH analysis software employing a finite-difference formula to calculate sub-pixel displacement. Using DFT as standard common formulation, I brought the two measurement approaches into near agreement. The finite-

 https://doi.org/10.37896/pd91.4/91459

ISSN: 0369-8963

difference approach measures velocity and acceleration at the sub-pixel level. This approach measures acceleration using the second derivative of a four-step central parabolic fit. Because it is less susceptible to location uncertainty, the second derivative of parabolic curve fitting detects acceleration with more precision than other techniques. [25, 26]

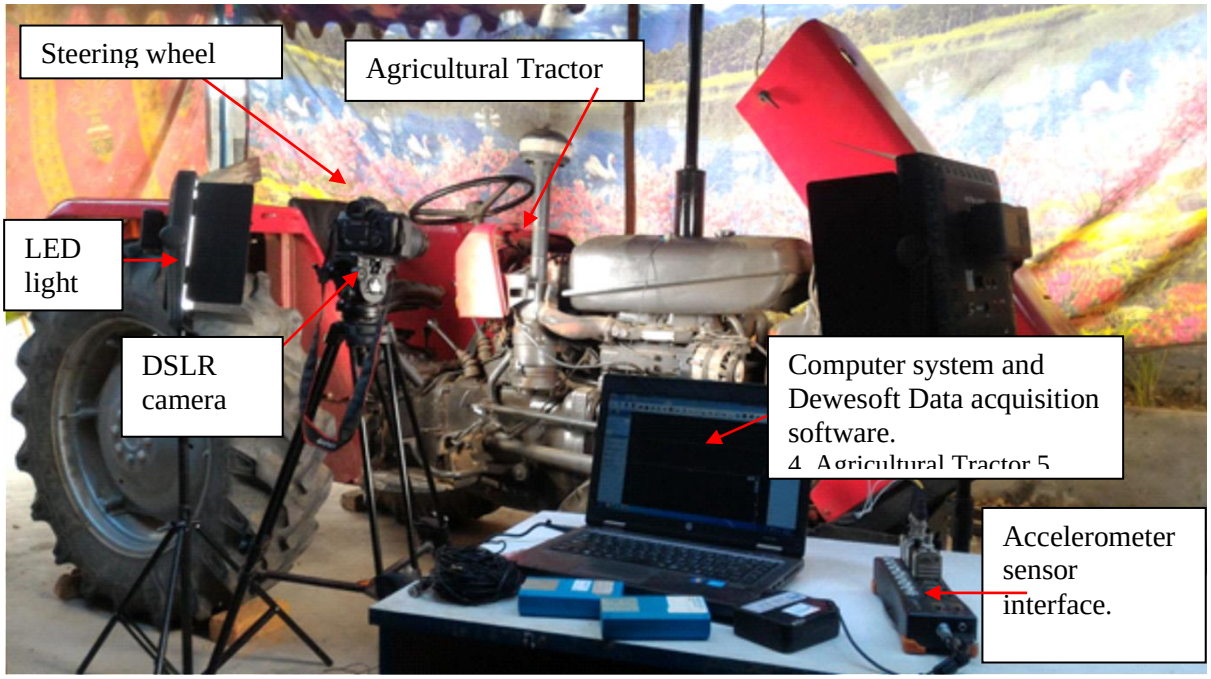

Figure 1: Experiment test setup

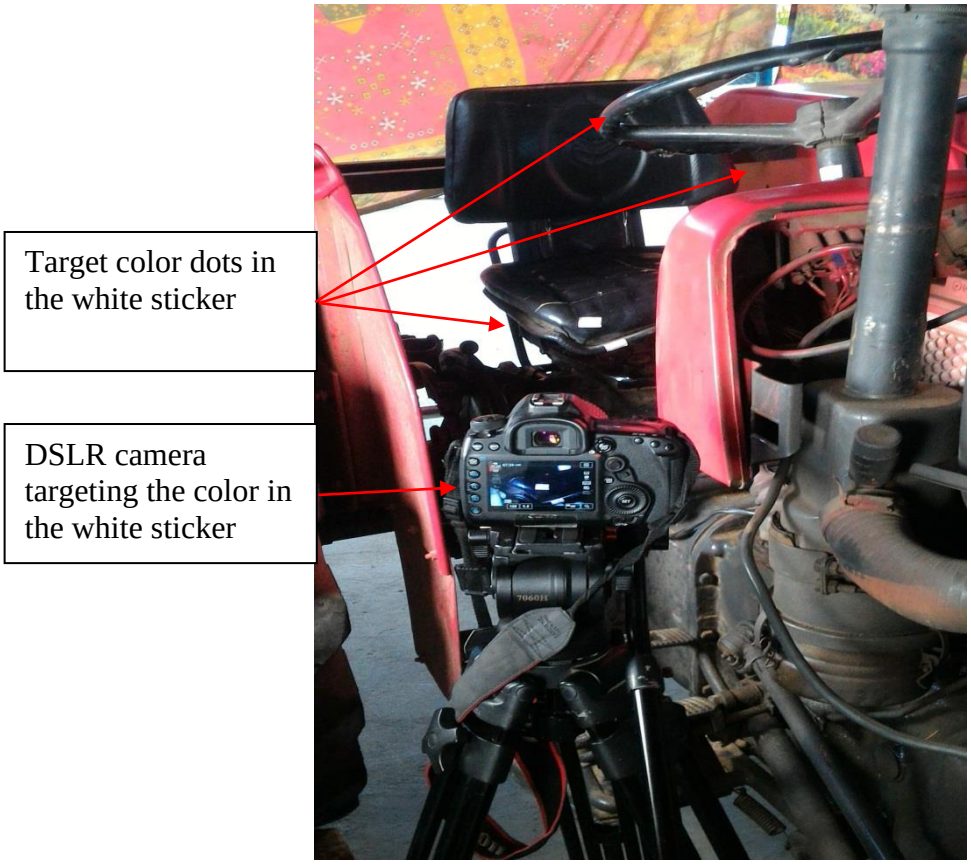

Figure 2: Closer view of the experimental test setup

https://doi.org/10.37896/pd91.4/91459

ISSN: 0369-8963

Experimental Method

Canon Eos 5D Mark II DSLR delivers 1920x1080, 640x480 at 30fps. In a 1920 1080 image, the lower right corner is at (1920,1080) pixels and the top left corner is at (0.0, 0.0). Figures 1 and 3 demonstrate the initial setup for determining image-to-world dimensions. A camera picture object's world coordinates are in metres to the reference frame. The known dimension paper sticker will be used as a reference for all video frames.

The coordinate system specifies each video frame and relates image dimensions to world coordinates. The scale (image unit per world unit) is the known height of the paper sticker, and the origin is the reference frame's image position. Mean RGB brightness in ROI was measured as a function of time to track the blue colour point in the video frames. The template match changes colour and shape at a set interval. Shorter template tracking intervals induce fast changes that can cause measurement drift.

By producing one or more template pictures in the ROI, a template matching algorithm traces the target location. The template image matches two successive images. The best template match is attained when the sum of the RGB squares is recorded as the maximum pixel difference. Interpolating the maximum and close match scores produces the sub-pixel match position of two picture frames. The x- and y-axis structural displacements were tabulated at the end of the template matching process. [25, 26]

Experimental Method

Canon Eos 5D Mark II DSLR delivers 1920x1080, 640x480 at 30fps. In a 1920 1080 image, the lower right corner is at (1920, 1080) pixels and the top left corner is at (0.0, 0.0). Figures 1 and 3 demonstrate the initial setup for determining image-to-world dimensions. A camera picture object's world coordinates are in meters to the reference frame. It will use the known dimension paper sticker as a reference for all video frames.

The coordinate system specifies each video frame and relates image dimensions to world coordinates. The scale (image unit per world unit) is the known height of the paper sticker, and the origin is the reference frame's image position. It measured mean RGB brightness in ROI as a function of time to track the blue colour point in the video frames. The template match changes colour and shape at a set interval. Shorter template tracking intervals induce fast changes that can cause measurement drift.

By producing one or more template pictures in the ROI, a template matching algorithm traces the target location. The template image matches two successive images. It attained the best template match when the sum of the RGB squares was recorded as the maximum pixel difference. Interpolating the maximum and close match scores produces the sub-pixel match position of two picture frames. The x- and y-axis structural displacements tabulated at the end of the template matching process. [25, 26]

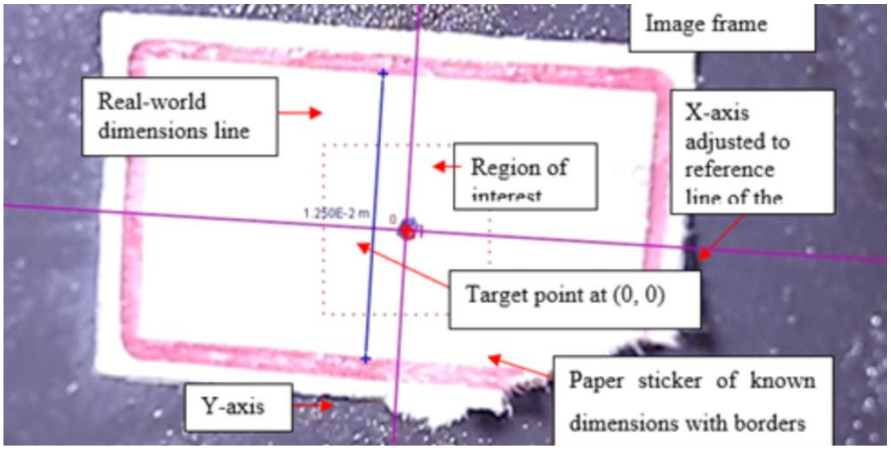

Figure 3: The x and y axes are set to (0, 0) at the target of ROI

https://doi.org/10.37896/pd91.4/91459

ISSN: 0369-8963

Fig. 3 shows a paper sticker with a real-world dimension. Keeping one axis parallel to the sticker's edge changed the image's tilt. The search region limits the template search. Target describes a blue point's position relative to the template during matching. Track points automate target point tracking.

RESULTS AND DISCUSSION

This machine vision system measured the vibration. TAFE tractor components were field-tested, and it correlated the results. It computed the displacement and acceleration data using an IEPE accelerometer, a SIRIUS® MINI interface, and Dewesoft NVH analysis software. It utilised a mathematical process to determine displacement and acceleration from video image frames, and the results were in good agreement.

The sub-pixel value derived from template matching using Up sampled Cross-Correlation to calculate displacement in pixels per millimetre. The finite-difference method computers velocity and acceleration at the sub-pixel level. The machine vision system investigated displacement calculation methods from target images. Using a finite element analysis, it compared the steering wheel outcomes of forklifts to the motion of a grating ruler. The accuracy of the changed Taylor approximation method and the Up-Sampled Cross-Correlation algorithm (UCC) with a hundred sample rate is extremely similar, but the changed Taylor approximation algorithm processes image frames 15 times faster than UCC. [25, 26]

Table 1: Comparison of vibration data in the X-direction and the Y-direction for 2 seconds

Frame Number	Time in Seconds	Pixel Value in X axis	Displacement in X axis in meter	Acceleration in X axis in meter(m/s^2) by Machine Vision System	Acceleration in X axis in meter (m/s^2) by Accelerometer.	Pixel Value in Y axis	Displacement in Y axis in meter	Acceleration in Y axis in meter (m/s^2) by Machine Vision System	Acceleration in Y axis in meter(m/s^2) by Accelerometer.
0	0	645.50000	0.00000		36.20000	362	1.39E-17		-0.01481
1	0.04	643.29240	-0.00026		3.60485	360.4852	0.00029		-0.01059
2	0.08	642.43570	-0.00032	0.10940	3.58972	358.9722	0.000533	-0.17898	-0.00414
3	0.12	643.39270	-0.00018	0.07356	3.58622	358.6215	0.000549	-0.11023	-0.02593
4	0.16	646.06190	0.00007	-0.02907	3.62215	362.2148	-5E-05	0.055632	0.020038
5	0.2	648.14300	0.00037	-0.17264	3.62176	362.1759	-0.00012	0.162952	0.032228
6	0.24	647.78150	0.00033	-0.12193	3.61827	361.8265	-5.6E-05	0.063692	0.004034
7	0.28	643.66570	-0.00023	0.06038	3.61080	361.0802	0.000194	0.06667	0.004237
8	0.32	642.45140	-0.00036	0.21847	3.59994	359.9938	0.000389	0.101321	0.068191
9	0.36	643.53000	-0.00027	0.10662	3.61750	361.7497	0.000104	-0.07903	-0.02378
10	0.4	647.41570	0.00029	-0.04853	3.61335	361.3346	2.62E-05	-0.02317	-0.01071
11	0.44	649.53950	0.00052	-0.12692	3.63299	363.2988	-0.00032	0.039019	0.018479
12	0.48	649.46060	0.00051	-0.04715	3.63451	363.451	-0.00034	0.047197	0.00385
13	0.52	649.31930	0.00048	0.00336	3.63668	363.6684	-0.00037	-0.00138	-0.04623
14	0.56	649.26260	0.00045	0.02076	3.64271	364.2714	-0.00045	-0.05405	-0.05244
15	0.6	649.28050	0.00045	-0.00473	3.64251	364.251	-0.00045	0.010472	0.00157
16	0.64	649.37380	0.00052	0.00136	3.62558	362.5575	-0.00021	-0.00344	-0.03921
17	0.68	649.20010	0.00043	-0.01264	3.64434	364.4344	-0.00047	-0.0334	-0.02838
18	0.72	649.37040	0.00053	0.00153	3.62487	362.4868	-0.0002	-0.00036	-0.02257
19	0.76	649.13060	0.00044	0.00607	3.64077	364.0774	-0.00042	-0.00922	-0.00054
20	0.8	649.21600	0.00045	0.00545	3.64158	364.1575	-0.00043	-0.0148	-0.00985

 https://doi.org/10.37896/pd91.4/91459

ISSN: 0369-8963

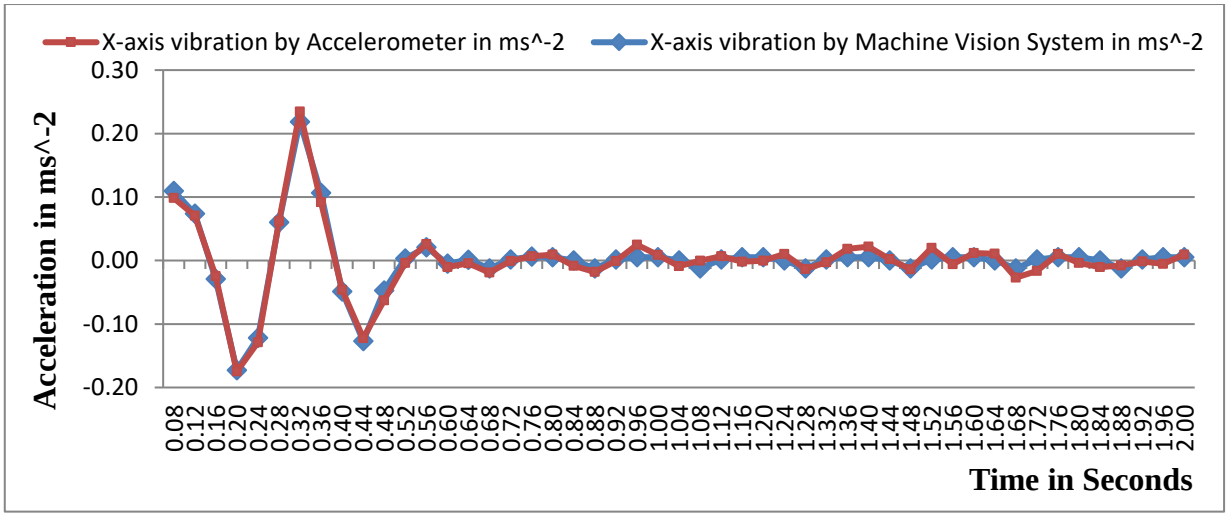

Figure 4: Vibration comparison for two seconds on X-axis (0.00 to 2.00 s)

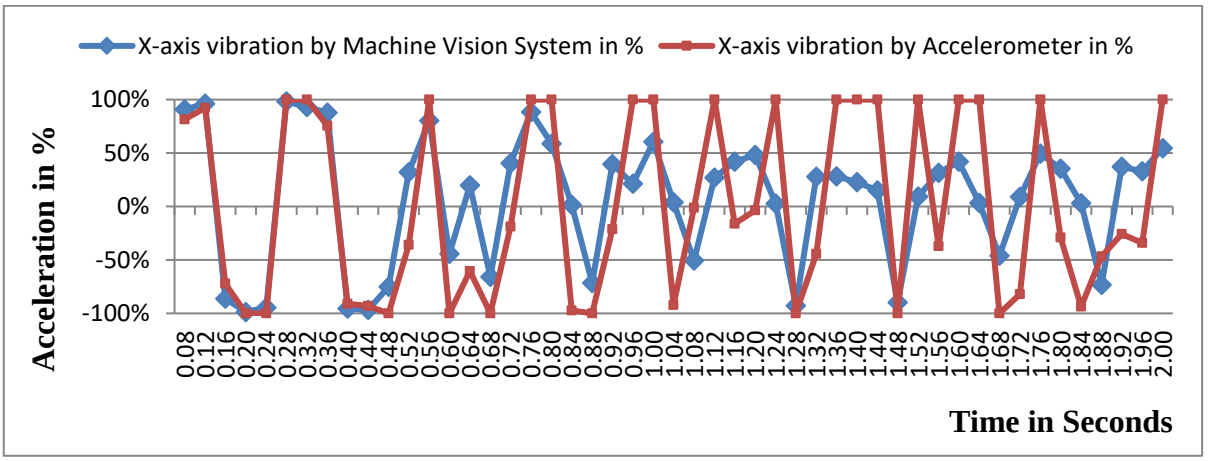

Figure 5: Percentage of Error Vibration comparisons for two seconds (0.00 to 2.00 s)

Figs.4 and 5 Show vibration amplitudes compared to two seconds. The maximum positive amplitude is recorded at 0.32 seconds with 4% error and the maximum negative amplitude is at 0.20 seconds with 2% error. It recorded the highest percentage of error at 0.64, 1.32 and 1.40 seconds, with an error of 30% to 50% at low vibration amplitude, which is not a necessary limit for vibration analysis. It recorded a maximum error between 0.001 and 0.005 ms^{-2} at low acceleration values.

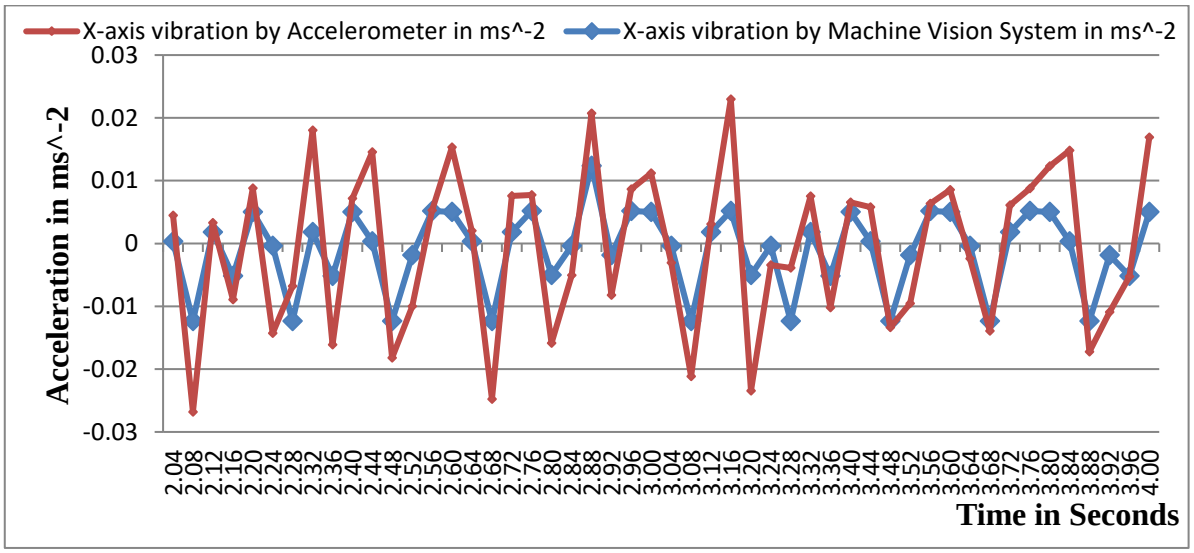

Figure 6: Vibration comparison for two seconds on X-axis (2.04 to 4.00 s)

https://doi.org/10.37896/pd91.4/91459

ISSN: 0369-8963

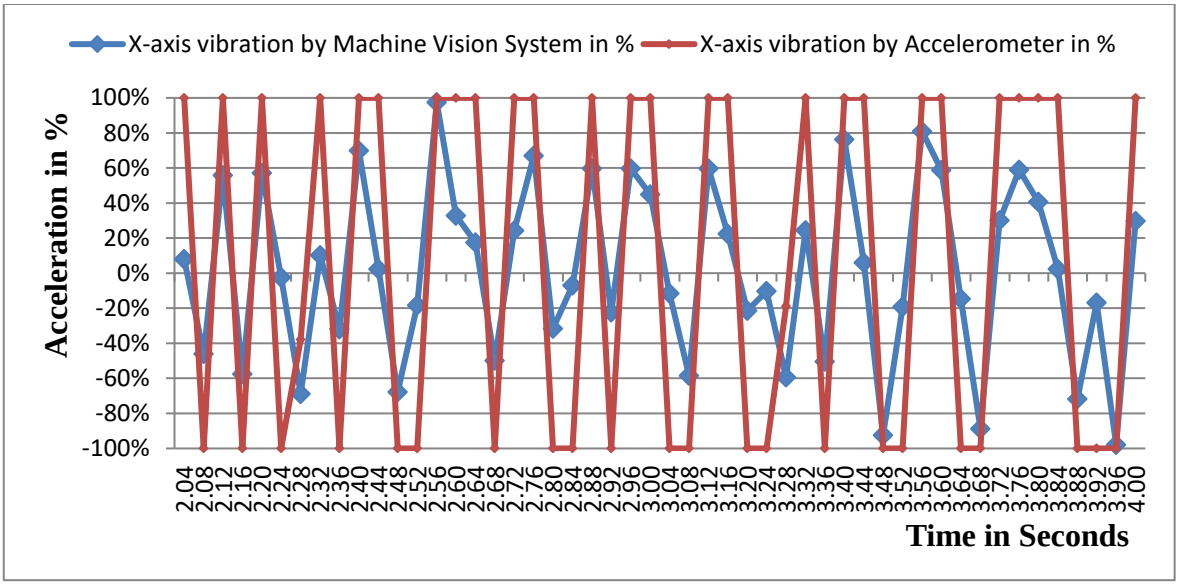

Figure 7: Percentage of Error Vibration comparisons for two seconds (2.04 to 4.00 s)

Figs.6 and 7 Show vibration amplitudes compared to two seconds. The maximum positive amplitude is recorded at 2.92 seconds with 10% error and the maximum negative amplitude is at 2.08 seconds with 10% error. It recorded the highest percentage of error at 2.68, 3.32 and 3.52 seconds, with an error of 30% to 50% at low vibration amplitude, which is not a necessary limit for vibration analysis. It recorded a maximum error between 0.001 and 0.005 ms^{-2} at low acceleration values.

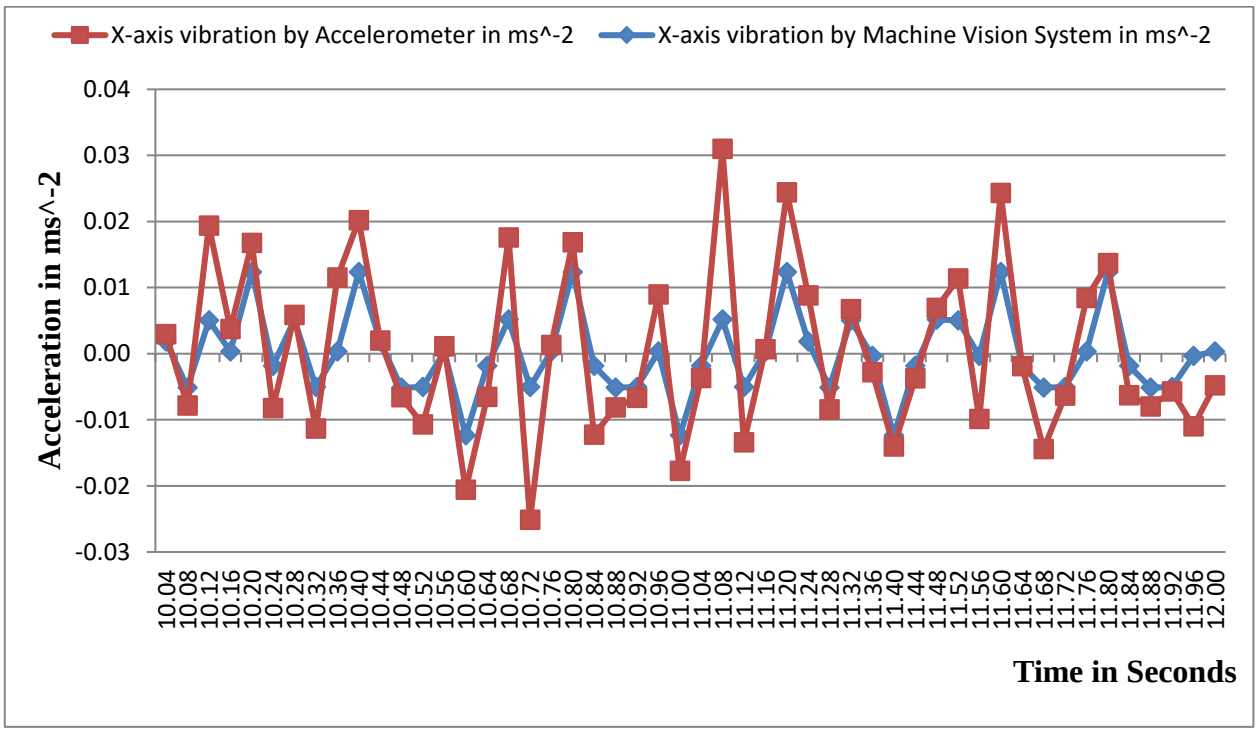

Figure 8: Vibration comparison for two seconds on X-axis (10.04 to 12.00 s)

Figs. 8 and 9 Show vibration amplitudes compared to two seconds. The maximum positive amplitude is recorded at 11.08 seconds with 50% error and the maximum negative amplitude is at 10.72 seconds with 50% error at high amplitude. In the entire one minute duration 1440 frame are analysed, this percentage of error is recorded high in this study.

https://doi.org/10.37896/pd91.4/91459

ISSN: 0369-8963

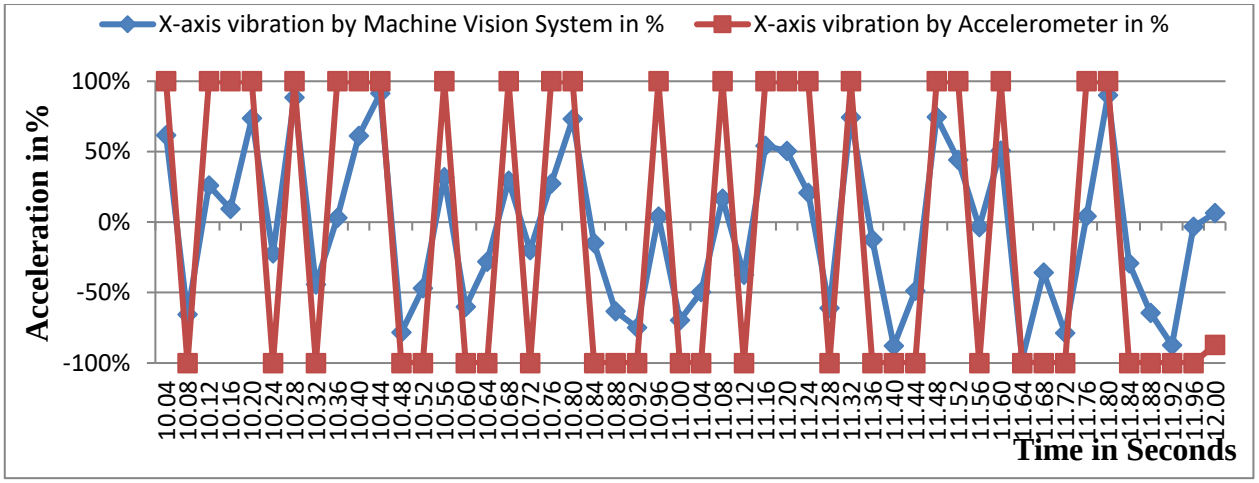

Figure 9: Percentage of Error Vibration comparisons for two seconds (10.04 to 12.00 s)

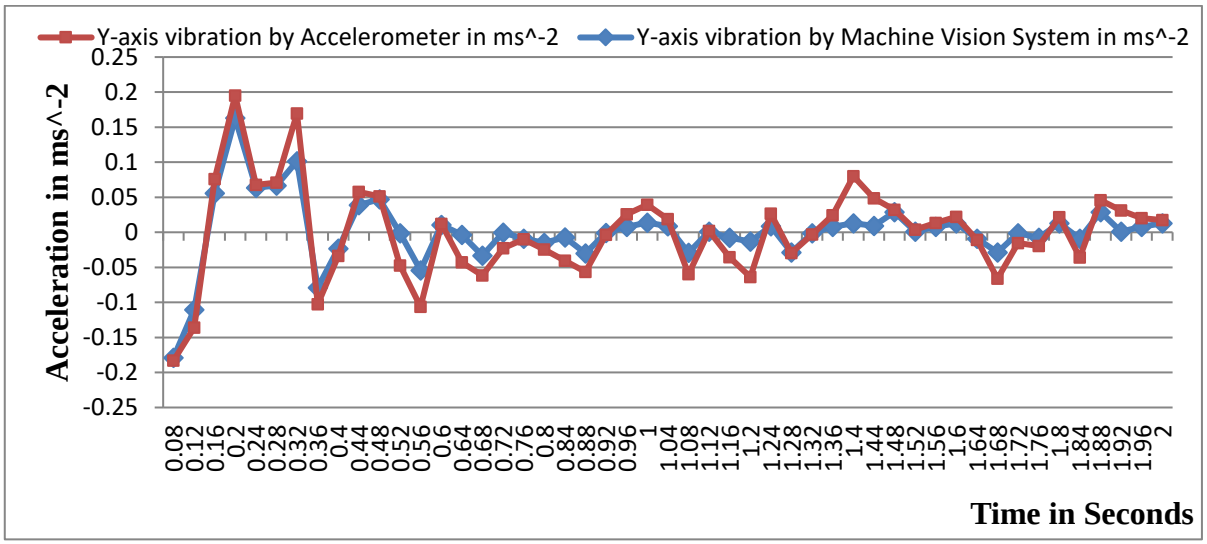

Figure 10: Vibration comparison for two seconds on Y-axis (08.00 to 2.00 s)

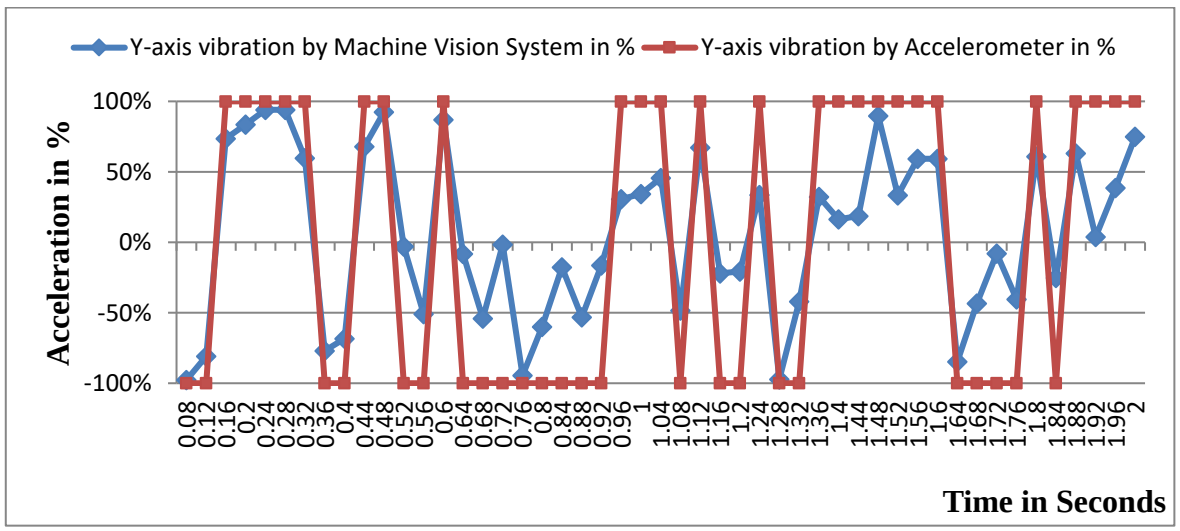

Figure 11: Percentage of Error Vibration comparisons for two seconds (0.00 to 2.00 s)

Figs.10 and 11 Show vibration amplitudes compared to two seconds. The maximum positive amplitude is recorded at 0.08 seconds with 2% error and the maximum negative amplitude is at 0.16 seconds with 5% error. It recorded the highest percentage of error at 0.84, 1.16 and 1.44 seconds, with an error of 30% to 50% at low vibration amplitude, which is not a necessary limit for vibration analysis. It recorded a maximum error between 0.001 and 0.005 ms^{-2} at low acceleration values.

https://doi.org/10.37896/pd91.4/91459

ISSN: 0369-8963

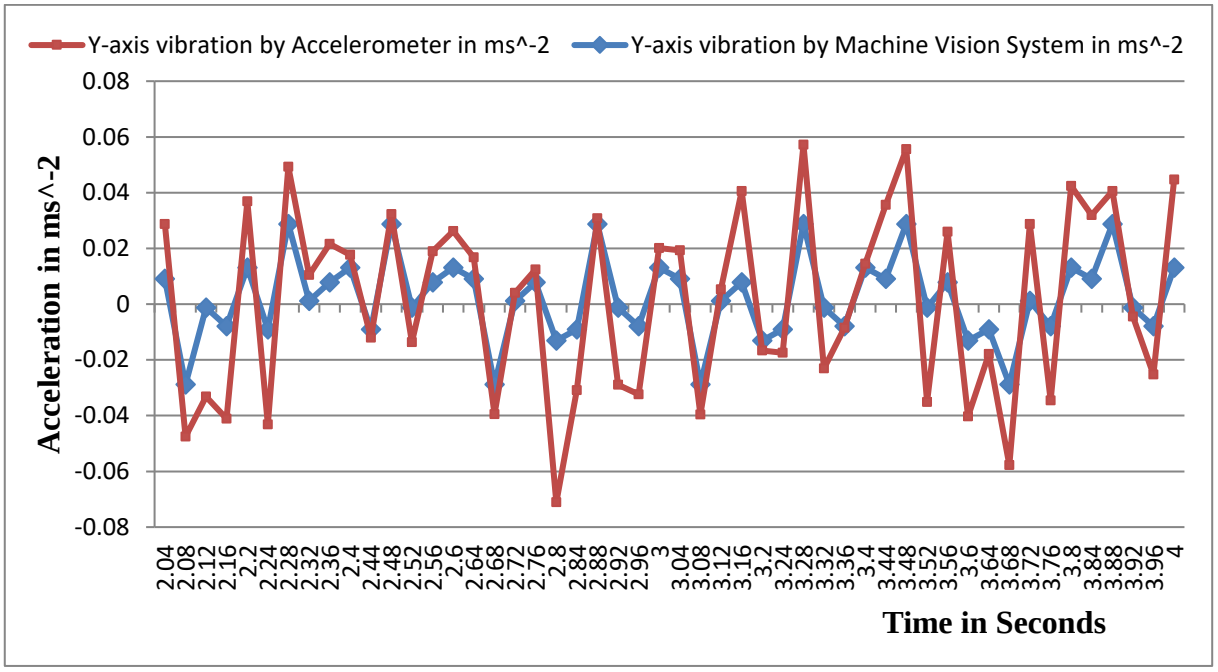

Figure 12: Vibration comparison for two seconds on Y-axis (2.04 to 4.00 s)

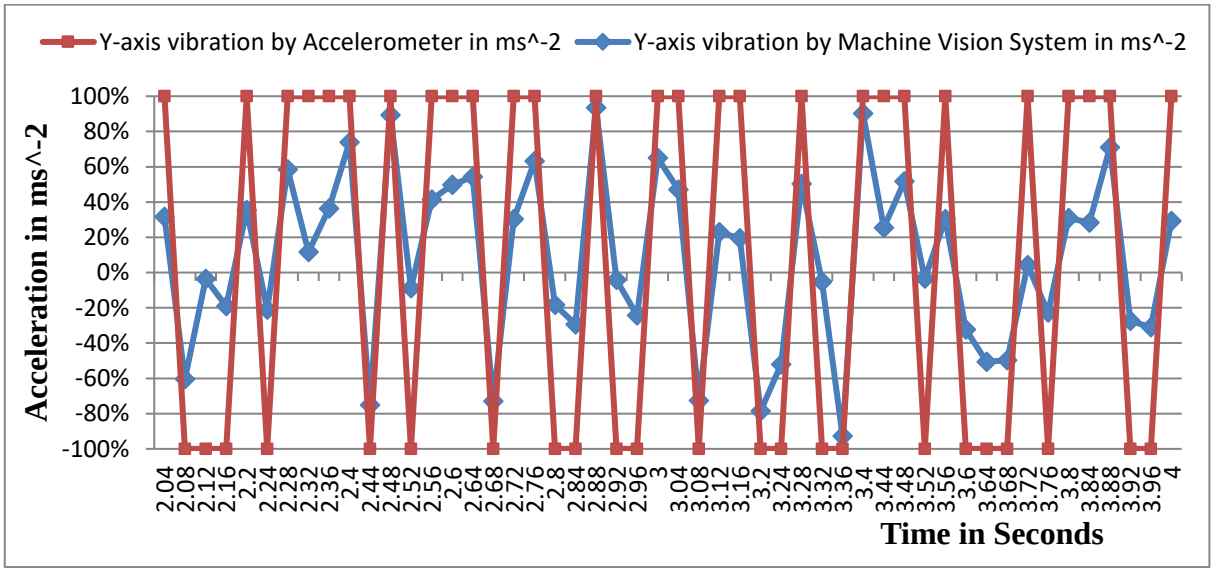

Figure 13: Percentage of Error Vibration comparisons for two seconds (2.04 to 4.00 s)

Figs.12 and 13 Show vibration amplitudes compared to two seconds. The maximum positive amplitude is recorded is at 3.2 seconds with 10% error and the maximum negative amplitude is at 2.8 seconds with 20% error. It recorded the highest percentage of error at 2.52, 3.32 and 3.72 seconds, with an error of 30% to 50% at low vibration amplitude, which is not a necessary limit for vibration analysis. It recorded a maximum error between 0.001 and 0.005 ms^{-2} at low acceleration values.

Figs.14 and 15 indicate vibration amplitudes compared to two seconds. It records the maximum positive amplitude is at 8.12 seconds with 10% error and the maximum negative amplitude is at 8.16 seconds with 20% error. It recorded the highest percentage of error is at 9. 2, 9.68 and 9.84 seconds, with an error of 30% to 50% at low vibration amplitude, which is not a necessary limit for vibration analysis. The maximum error was between 0.001 and 0.005 ms^{-2}. It noted that there is data retrieval by the Machine vision system at the time of 9.36s, 9.4s, 9.48s and 9.56s. The template algorithm did not able to the point in the above said frames; actual reason is to be studied.

https://doi.org/10.37896/pd91.4/91459

ISSN: 0369-8963

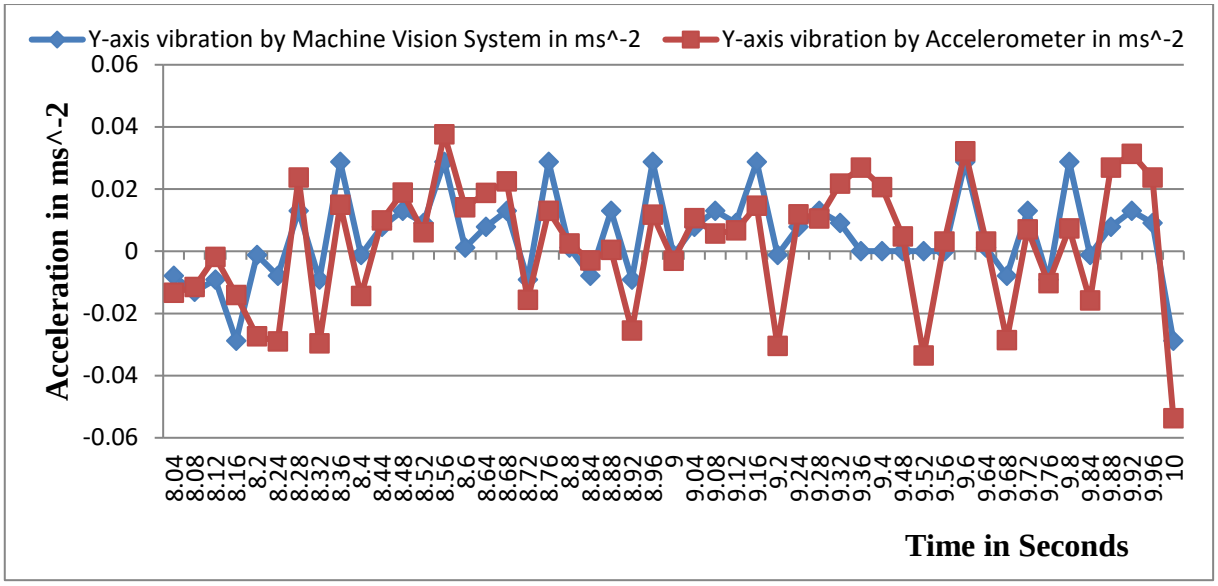

Figure 14: Vibration comparison for two seconds on Y-axis (8.04 to 10.00 s)

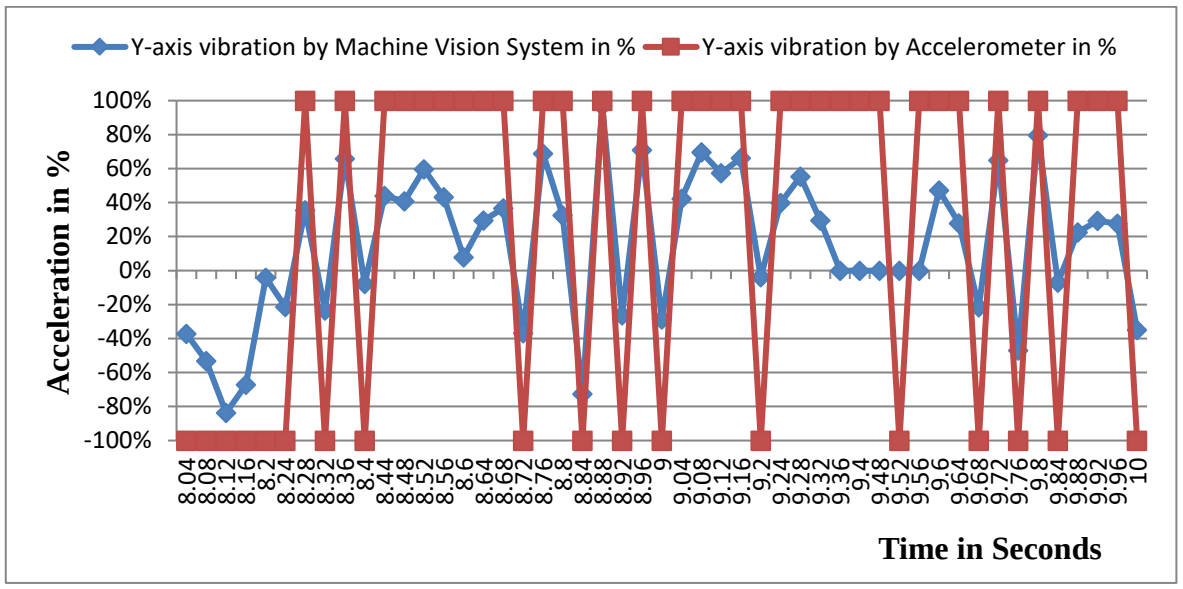

Figure 15: Percentage of Error Vibration comparisons for two seconds (8.04 to 10.00 s)

The references [25, 26, 30-43] validate the sensor and algorithm of the proposed vision system. The sources [41 and 42] validate the outcomes and percentage of error. The proposed system displays the same error pattern. For smaller displacement values, the proportion of inaccuracy is greater; for bigger displacement values, it is comparable. This proposed machine vision system can measure a minimum displacement of 0.01 mm.

CONCLUSION

The proposed study is an optimized system for vibration measurement in stationary machines with low frequency. The macro lens used in this experiment captures a specific target closely and has a specific aspect ratio for magnifying that image. In order for the machine mission process to be accurate, the noises in the image should be low. Taking this into account, a white sticker with previously known measurements was used to reduce the background noises. Taking the colored dot on this white sticker as a target, the template matching algorithm compares the reference frame to other frames and calculates the movement of a dot. The calculated vibration levels are compared with the measurements obtained from the accelerometer, which calculate the vibrations in the traditional way, and confirm a close correlation between the two. The videos captured in machine vision technology

 https://doi.org/10.37896/pd91.4/91459

ISSN: 0369-8963

easily transmitted to computers and analyzed, so this method is suitable for industrial automation technology called Industry 4.0 and in this method drawbacks in traditional vibration measuring instruments avoided and it save time and money.

When analyzing the obtained results, the results show that when the vibration is high; the errors are less and when the vibration is low, near zero, the errors range from 30 percent to 50 percent. But this study suggests that very low-level vibrations are unnecessary for vibration analysis and therefore should not be considered. This study is not suitable for Nano-vibration measurement methods that measure fine vibrations.

In this study, it was impossible to calculate vibration in three axes from the video images recorded by the camera. According to ISO 5349-2, the vibration obtained on two axes multiplied by 1 to 1.7 to calculate the equivalent measurement for the vibration on the third axis. So with this machine vision method the vibration in agricultural tractor steering wheel calculated, by this, the total frequency weighted value can be calculated equal to 8 hours using the formula given in equation two. Comparing this calculated weighted frequency value with the eight-hour equivalent exposure listed in ISO 5349-1, 2001. By comparison, it is possible to know how and to what extent the driver's hand has affected by the vibration through the tractor steering wheel, the vibration can be reduced by taking appropriate pre-maintenance measures, or the driver's hands can be protected from vibration-related diseases by ensuring that the working hours do not exceed a certain limit.

REFERENCES

[1] "Mechanical Vibration – Measurement and Evaluation of Human Exposure to Hand Transmitted Vibration, Part 1: General Requirements [MED 28: Mechanical Vibration and Shock," BUREAU OF INDIAN STANDARDS, IS/ISO 5349-1 (2001) vol.1 pp.1-24, 2007

[2] S. Gnanasekaran, M. Ajovalasit and J. Giacomin, "Driver estimation of steering wheel vibration intensity laboratory-based tests," Engineering Integrity, Vol. 20, pp. 25-31, 2006

[3] B. Cvetanovic and D. Zlatkovic, "Evaluation of Whole-Body Vibration Risk in Agricultural Tractor Drivers Tractor Drivers," Bulgarian Journal of Agricultural Science, vol.19 (No 5), pp.1155-1160, 2013

[4] M. Morioka and M.J. Griffin, "Frequency dependence of perceived intensity of steering wheel vibration: effect of grip force," Proceedings of Second Joint EuroHaptics Conference and Symposium on Haptic Interfaces for Virtual Environment and Teleoperator Systems (WHC'07), vol. 1, pp. 50-55, 2007.

[5] S.A. A. Aziz, M.Z. Nuawi and M. J. Mohd Nor, "New regression model for predicting hand-arm vibration (HAV) of Malaysian Army (MA) three-tonne truck steering wheels," Journal of Occupational Health, vol.57, pp. 513–520, 2015

[6] S. A. Ab Aziz, M. Z. Nuawi and M. J. Mohd Nor "Monitoring of hand-arm vibration," International Journal of Acoustics and Vibration, Vol. 22, No. 1, pp. 34-43, 2017

[7] R. Janczur, "Proposal to use vibration analysis steering components and car body to monitor, for example, the state of unbalance wheel," IOP Conference Series: Materials Science and Engineering, vol.148, pp. 1-10, 2016.

[8] T. Tang, S. He, M. Ye, E. Xu and W. Zheng ," Research on a Multinode Joint Vibration Control Strategy for Controlling the Steering Wheel of a Commercial Vehicle," Shock and Vibration, Vol. 2020, pp. 1-21, 2020.

[9] M.Wandor and R.Burdzik, "Research on vibration of steering gear of automotive vehicle," VibroEngineering Procedia, Vol. 6, pp. 264-267, 2015.

[10] S. He, T. Tang, E. Xu, M. Ye and W. Zheng, "Vibration control analysis of vehicle steering system based on combination of finite-element analysis and modal testing," Journal of Vibration and Control, vol. 26(1–2), pp. 88–101, 2020

 https://doi.org/10.37896/pd91.4/91459

ISSN: 0369-8963

[11] A. A.A. H. AL-Mafrachi, “Whole body, arm-hand vibration and performance drivers tractors during conservation tillage under different velocity and soils,” International Journal of Advanced Engineering, Management and Science, vol-2(1), pp1-14, 2016.
[12] P. A. Savta and P. H. Jain, “A study of reduction in the vibrations of steering wheel of agricultural tractor,” Int. Journal of Engineering Research and Application, vol. 6(10), pp.80-87, 2016.
[13] S. He, T. Tang, M. Ye, E. Xu and Z. Jiang, "A Multi-Point Iterative Analysis Method for Vibration Control of a Steering Wheel at Idle Speed," IEEE Access, vol. 7, pp. 88399-88417, 2019.
[14] A.A.A.Hamid, M. K.Abdullah, A. A.H. Ali, and A. F. Fahem, “Effect of steering wheel vibration on drivers hands in a two-wheel drivers hand tractor,” Journal of Engineering, vo.17, pp. 1079-1087, 2011.
[15] P.B. Shelke1, A. D. Dhale, “Experimental analysis for the vibration reduction of steering wheel assembly of agricultural tractor,” Conference on technologies for future cities (CTFC), vol.1, pp. 1-6, 2019.
[16] G. Prashanth, P. K.Patro and Dr. Velamurali, “Mathematical modeling of vibration in steering wheel assembly of commercial vehicles,” International Journal of Engineering Research & Technology, vol. 4 (04), pp. 837-841, 2015.
[17] C.Zhang, H.Ao and H. Jiang, “Vibration analysis and experimental research on metal rubber vibration isolation of vehicle steering wheel,” IOP Conf. Series: Materials Science and Engineering, vol. 397, pp. 1-6, 2018.
[18] T.Wang , Y. Wang, L. Zhu, Z. Zhi, Z. Liu and R. Li, “Research on Steering Vibration Analysis of Wheel Loader and Cushion Valve Design” , Energies, vol. 805, pp.1-15, 2022.
[19] S. Cankaya, A. Koyuncu and M. Balaban, “Steering Wheel Idle Vibration Improvement on Tractor,” Sigma Journal Engineering and Natural Sciences, vol. 34 (1), pp. 91-103, 2016.
[20] V. Balambica and V.Deepak, “Study and Analysis of Reducing Hand Vibration in a Tractor ,” International Journal of Pure and Applied Mathematics, vol. 116 no. 18, pp. 275-279, 2017.
[21] N.Manish, “Study of Vibrations on Steering Wheel Study of Vibrations on Steering Wheel- A Review” Journal of Chemical and Pharmaceutical Sciences, vol.5, pp.412-415, 2016.
[22] A. Shinde and S. G. Jadhav, “Vibration Measurement and Vibration Reduction of Steering Wheel of an Agricultural Tractor,” International Journal of Science and Research, vol. 5(7), pp.44-48, 2016.
[23] A. Peretti, E. Carletti, F. Pedrielli, J. Griguolo , F. Pompoli and et al. “Vibration Tests on Five Agricultural Tractors with Increasingly Efficient Vibration Control Systems under Normal Working Conditions,” Annual Congress of the International Institute of Acoustics and Vibration (IIAV), vol. 1, pp. 1-8, 2021.
[24] P. B. Magade, P. P. Deshattiwar and K. L. Bhoite, “Vibrational analysis of carbon fiber steering wheel,” International Journal of Advance Research, Ideas and Innovations in Technology, vol. 5(3), pp.1561-1566, 2019.
[25] R. Ganesan, Dr.G.Sankaranarayanan, Dr.M.Pradeep Kumar, Dr.V.K.Bupesh Raja "Vibration-Based Condition Monitoring of a Tractor Radiator using Machine Vision System," International Journal of Engineering Trends and Technology, vol. 70.1,pp.283-290, 2022.
[26] R. Ganesan, G. Sankaranarayanan, M. Pradeep Kumar and V. K. Bupesh Raja, “Up-Sampled Cross-Correlation Based Object Tracking & Vibration Measurement in Agriculture Tractor System,” Intelligent Automation & Soft Computing, vol.prepress, pp.1-15, 2022.
[27] P. Pathmanaban, B.K. Gnanavel and A. Shanmuga Sundaram , “Damage Detection and Classification of Mangoes Based on Thermal Imaging,” PERIODICO di MINERALOGIA Volume 91, No. 3, pp.270-278, 2022.
[28] C.Z.Dong, S.Bas and N. A. Catbas, “Completely Non-Contact Recognition System for Bridge Unit Influence Line Using Portable Camerasand Computer Vision,” Smart Structures and Systems, vol. 24, pp.no 617–630, 2019.
[29] R. Zaurin and F.N. Catbas, “Structural Health Monitoring using Video Stream, Influence Lines, and Statistical Analysis,” Structural Control and Health Monitoring , vol. 10, pp. 309–332, 2010.
[30] Y. Fukuda, M.Q. Feng, Y. Narita, S. Kaneko. T. Tanaka, “Vision-based displacement sensor for monitoring dynamic response using robust object search algorithm,” IEEE Sensors Journal, vol.13, pp. 4725–4732, 2013.

 https://doi.org/10.37896/pd91.4/91459

ISSN: 0369-8963

[31] Y.F. Ji, "A computer vision-based approach for structural displacement measurement. In Proceedings of the Conference on Sensors and Smart Structures Technologies for Civil, Mechanical, and Aerospace Systems" SPIE - The International Society of Optics and Photonics, vol.1 pp.1-8, 2010.
[32] A. Shariati and T. Schumacher, "Eulerian-based virtual visual sensors to measure dynamic displacements of structures," Structural Control and Health Monitoring, 2017, vol. 24, pp.1977, 2017.
[33] H.Yoon, H. Elanwar, H. Choi, M.Golparvar-Fard, and B.F. Spencer Jr. "Target-free approach for vision-based structural system identification using consumer-grade cameras," Structural Control and Health Monitoring, vol. 23, pp.1405–1416, 2016.
[34] M.A. Kuddus, J.Li, H. Hao, , C. Li and K. Bi, "Target-free vision-based technique for vibration measurements of structures subjected to out-of-plane movements," Engineering Structures, vol.190, pp. 210–222,2019.
[35] A. Cigada, P. Mazzoleni, and E. Zappa, "Vibration Monitoring of Multiple Bridge Points by Means of a Unique Vision-Based Measuring System," Experimental Mechanics, vol.54, pp. 255–271, 2014.
[36] G.A.Stephen, J.M.W. Brown john and C.A. Taylor, "Measurements of static and dynamic displacement from visual monitoring of the Humber Bridge," Engineering Structures, vol. 15, pp.197–208, 1993.
[37] J.H.G. Macdonald, E.L. Dagless, B.T.Thomas and C.A. Taylor, "Dynamic measurements of the second severn crossing" Proceedings of the Institution of Civil Engineers – Transport, vol. 123, pp.241–248, 1997.
[38] Z. Zhang, "A flexible new technique for camera calibration," IEEE Transactions on Pattern Analysis and Machine Intelligence, vol. 22, pp.1330–1334, 2000.
[39] B. Liu, D. Zhang, J. Guo and C. Zhu, "Vision-based displacement measurement sensor using modified Taylor approximation approach," Optical Engineering, vol. 55, no. 11, pp. 114103-10, 2016.
[40] D. Feng, M. Q. Feng, E. Ozer and Y. Fukuda, "A Vision-based sensor for noncontact structural displacement measurement," Sensors, vol. 15, no. 7, pp. 16557–16575, 2015.
[41] J. Lee, K. -C. Lee, S. Cho and S. -H. Sim, "Computer vision-based structural displacement measurement robust to light-induced image degradation for in-service bridges," Sensors, vol. 17, pp. 2317, 2017.
[42] J. Javh, J. Slavic and M. Boltezar, "Measuring full-field displacement spectral components using photographs taken with a DSLR camera via an analogue Fourier integral," Mechanical Systems and Signal Processing, vol. 100, pp. 17–27, 2018.
[43] M. Yang, C. Cai, Y. Wang, H. Zhu and Z. Liu, "A novel low frequency vibration measurement method based on single camera," Journal of Physics, Conference Series, pp. 1065, 2018.

 https://doi.org/10.37896/pd91.4/91459